Featured in Physics

Properties of Iron Primary Cosmic Rays: Results from the Alpha Magnetic Spectrometer

M. Aguilar,[30] L. Ali Cavasonza,[1] M. S. Allen,[10] B. Alpat,[37] G. Ambrosi,[37] L. Arruda,[28] N. Attig,[24] F. Barao,[28] L. Barrin,[15] A. Bartoloni,[43] S. Başeğmez-du Pree,[18,*] R. Battiston,[40,41] M. Behlmann,[10] B. Beischer,[1] J. Berdugo,[30] B. Bertucci,[37,38] V. Bindi,[20] W. de Boer,[25] K. Bollweg,[21] B. Borgia,[43,44] M. J. Boschini,[32] M. Bourquin,[16] E. F. Bueno,[18] J. Burger,[10] W. J. Burger,[40] S. Burmeister,[26] X. D. Cai,[10] M. Capell,[10] J. Casaus,[30] G. Castellini,[14] F. Cervelli,[39] Y. H. Chang,[48,49] G. M. Chen,[6,7] G. R. Chen,[23] H. S. Chen,[6,7] Y. Chen,[16,23] L. Cheng,[23] H. Y. Chou,[49] S. Chouridou,[1] V. Choutko,[10] C. H. Chung,[1] C. Clark,[10,21] G. Coignet,[3] C. Consolandi,[20] A. Contin,[8,9] C. Corti,[20] Z. Cui,[22,23] K. Dadzie,[10] C. Delgado,[30] S. Della Torre,[32] M. B. Demirköz,[2] L. Derome,[17] S. Di Falco,[39] V. Di Felice,[45,†] C. Díaz,[30] F. Dimiccoli,[40] P. von Doetinchem,[20] F. Dong,[35] F. Donnini,[45,†] M. Duranti,[37] A. Egorov,[10] A. Eline,[10] J. Feng,[10] E. Fiandrini,[37,38] P. Fisher,[10] V. Formato,[45,†] C. Freeman,[20] Y. Galaktionov,[10] C. Gámez,[30] R. J. García-López,[27] C. Gargiulo,[15] H. Gast,[1] M. Gervasi,[32,33] F. Giovacchini,[30] D. M. Gómez-Coral,[20] J. Gong,[35] C. Goy,[3] V. Grabski,[31] D. Grandi,[32,33] M. Graziani,[37,38] S. Haino,[48] K. C. Han,[29] R. K. Hashmani,[2] Z. H. He,[19] B. Heber,[26] T. H. Hsieh,[10] J. Y. Hu,[6,7] M. Incagli,[39] W. Y. Jang,[13] Yi Jia,[10] H. Jinchi,[29] K. Kanishev,[40] B. Khiali,[45,†] G. N. Kim,[13] Th. Kirn,[1] M. Konyushikhin,[10] O. Kounina,[10] A. Kounine,[10] V. Koutsenko,[10] A. Kuhlman,[20] A. Kulemzin,[10] G. La Vacca,[32,33] E. Laudi,[15] G. Laurenti,[8] I. Lazzizzera,[40,41] A. Lebedev,[10] H. T. Lee,[47] S. C. Lee,[48] J. Q. Li,[35] M. Li,[1] Q. Li,[35] S. Li,[1] J. H. Li,[22] Z. H. Li,[6,7] J. Liang,[22] C. Light,[20] C. H. Lin,[48] T. Lippert,[24] J. H. Liu,[5] Z. Liu,[16] S. Q. Lu,[48] Y. S. Lu,[6] K. Luebelsmeyer,[1] J. Z. Luo,[35] Xi Luo,[23] S. S. Lyu,[19] F. Machate,[1] C. Mañá,[30] J. Marín,[30] J. Marquardt,[26] T. Martin,[10,21] G. Martínez,[30] N. Masi,[8,9] D. Maurin,[17] A. Menchaca-Rocha,[31] Q. Meng,[35] V. V. Mikhailov,[34] D. C. Mo,[19] M. Molero,[30] P. Mott,[10,21] L. Mussolin,[37,38] J. Negrete,[20] N. Nikonov,[1] F. Nozzoli,[40] A. Oliva,[8] M. Orcinha,[28] M. Palermo,[20] F. Palmonari,[8,9] M. Paniccia,[16] A. Pashnin,[10] M. Pauluzzi,[37,38] S. Pensotti,[32,33] H. D. Phan,[10] R. Piandani,[25] V. Plyaskin,[10] S. Poluianov,[36] X. Qin,[10] Z. Y. Qu,[48] L. Quadrani,[8,9] P. G. Rancoita,[32] D. Rapin,[16] A. Reina Conde,[27] E. Robyn,[16] S. Rosier-Lees,[3] A. Rozhkov,[10] D. Rozza,[32,33] R. Sagdeev,[11] S. Schael,[1] A. Schulz von Dratzig,[1] G. Schwering,[1] E. S. Seo,[12] Z. Shakfa,[2] B. S. Shan,[4] T. Siedenburg,[1] C. Solano,[10] J. W. Song,[22] X. J. Song,[23] R. Sonnabend,[1] L. Strigari,[43,‡] T. Su,[23] Q. Sun,[22] Z. T. Sun,[6,7] M. Tacconi,[32,33] X. W. Tang,[6] Z. C. Tang,[6] J. Tian,[37,38] Samuel C. C. Ting,[10,15] S. M. Ting,[10] N. Tomassetti,[37,38] J. Torsti,[50] C. Tüysüz,[2] T. Urban,[10,21] I. Usoskin,[36] V. Vagelli,[42,37] R. Vainio,[50] M. Valencia-Otero,[49] E. Valente,[43,44] E. Valtonen,[50] M. Vázquez Acosta,[27] M. Vecchi,[18] M. Velasco,[30] J. P. Vialle,[3] C. X. Wang,[22] L. Wang,[5] L. Q. Wang,[22] N. H. Wang,[22] Q. L. Wang,[5] S. Wang,[20] X. Wang,[10] Yu Wang,[22] Z. M. Wang,[23] J. Wei,[16] Z. L. Weng,[10] H. Wu,[35] R. Q. Xiong,[35] W. Xu,[22,23] Q. Yan,[10] Y. Yang,[46] I. I. Yashin,[34] H. Yi,[35] Y. M. Yu,[19] Z. Q. Yu,[6] M. Zannoni,[32,33] C. Zhang,[6] F. Zhang,[6] F. Z. Zhang,[6,7] J. H. Zhang,[35] Z. Zhang,[10] F. Zhao,[6,7] C. Zheng,[23] Z. M. Zheng,[4] H. L. Zhuang,[6] V. Zhukov,[1] A. Zichichi,[8,9] N. Zimmermann,[1] and P. Zuccon[40,41]

(AMS Collaboration)

[1]*I. Physics Institute and JARA-FAME, RWTH Aachen University, 52056 Aachen, Germany*
[2]*Department of Physics, Middle East Technical University (METU), 06800 Ankara, Turkey*
[3]*Univ. Grenoble Alpes, Univ. Savoie Mont Blanc, CNRS, LAPP-IN2P3, 74000 Annecy, France*
[4]*Beihang University (BUAA), Beijing, 100191, China*
[5]*Institute of Electrical Engineering (IEE), Chinese Academy of Sciences, Beijing, 100190, China*
[6]*Institute of High Energy Physics (IHEP), Chinese Academy of Sciences, Beijing, 100049, China*
[7]*University of Chinese Academy of Sciences (UCAS), Beijing, 100049, China*
[8]*INFN Sezione di Bologna, 40126 Bologna, Italy*
[9]*Università di Bologna, 40126 Bologna, Italy*
[10]*Massachusetts Institute of Technology (MIT), Cambridge, Massachusetts 02139, USA*
[11]*East–West Center for Space Science, University of Maryland, College Park, Maryland 20742, USA*
[12]*IPST, University of Maryland, College Park, Maryland 20742, USA*
[13]*CHEP, Kyungpook National University, 41566 Daegu, Korea*
[14]*CNR–IROE, 50125 Firenze, Italy*
[15]*European Organization for Nuclear Research (CERN), 1211 Geneva 23, Switzerland*
[16]*DPNC, Université de Genève, 1211 Genève 4, Switzerland*
[17]*Univ. Grenoble Alpes, CNRS, Grenoble INP, LPSC-IN2P3, 38000 Grenoble, France*
[18]*Kapteyn Astronomical Institute, University of Groningen, P.O. Box 800, 9700 AV Groningen, Netherlands*

[19]Sun Yat–Sen University (SYSU), Guangzhou, 510275, China
[20]Physics and Astronomy Department, University of Hawaii, Honolulu, Hawaii 96822, USA
[21]National Aeronautics and Space Administration Johnson Space Center (JSC), Houston, Texas 77058, USA
[22]Shandong University (SDU), Jinan, Shandong, 250100, China
[23]Shandong Institute of Advanced Technology (SDIAT), Jinan, Shandong, 250100, China
[24]Jülich Supercomputing Centre and JARA-FAME, Research Centre Jülich, 52425 Jülich, Germany
[25]Institut für Experimentelle Teilchenphysik, Karlsruhe Institute of Technology (KIT), 76131 Karlsruhe, Germany
[26]Institut für Experimentelle und Angewandte Physik, Christian-Alberts-Universität zu Kiel, 24118 Kiel, Germany
[27]Instituto de Astrofísica de Canarias (IAC), 38205 La Laguna, and Departamento de Astrofísica, Universidad de La Laguna, 38206 La Laguna, Tenerife, Spain
[28]Laboratório de Instrumentação e Física Experimental de Partículas (LIP), 1649-003 Lisboa, Portugal
[29]National Chung–Shan Institute of Science and Technology (NCSIST), Longtan, Tao Yuan, 32546, Taiwan
[30]Centro de Investigaciones Energéticas, Medioambientales y Tecnológicas (CIEMAT), 28040 Madrid, Spain
[31]Instituto de Física, Universidad Nacional Autónoma de México (UNAM), Ciudad de México, 01000 Mexico
[32]INFN Sezione di Milano–Bicocca, 20126 Milano, Italy
[33]Università di Milano–Bicocca, 20126 Milano, Italy
[34]NRNU MEPhI (Moscow Engineering Physics Institute), Moscow, 115409 Russia
[35]Southeast University (SEU), Nanjing, 210096, China
[36]Sodankylä Geophysical Observatory and Space Physics and Astronomy Research Unit, University of Oulu, 90014 Oulu, Finland
[37]INFN Sezione di Perugia, 06100 Perugia, Italy
[38]Università di Perugia, 06100 Perugia, Italy
[39]INFN Sezione di Pisa, 56100 Pisa, Italy
[40]INFN TIFPA, 38123 Povo, Trento, Italy
[41]Università di Trento, 38123 Povo, Trento, Italy
[42]Agenzia Spaziale Italiana (ASI), 00133 Roma, Italy
[43]INFN Sezione di Roma 1, 00185 Roma, Italy
[44]Università di Roma La Sapienza, 00185 Roma, Italy
[45]INFN Sezione di Roma Tor Vergata, 00133 Roma, Italy
[46]National Cheng Kung University, Tainan, 70101, Taiwan
[47]Academia Sinica Grid Center (ASGC), Nankang, Taipei, 11529, Taiwan
[48]Institute of Physics, Academia Sinica, Nankang, Taipei, 11529, Taiwan
[49]Physics Department and Center for High Energy and High Field Physics, National Central University (NCU), Tao Yuan, 32054, Taiwan
[50]Space Research Laboratory, Department of Physics and Astronomy, University of Turku, 20014 Turku, Finland

(Received 2 October 2020; revised 22 November 2020; accepted 9 December 2020; published 28 January 2021)

We report the observation of new properties of primary iron (Fe) cosmic rays in the rigidity range 2.65 GV to 3.0 TV with 0.62×10^6 iron nuclei collected by the Alpha Magnetic Spectrometer experiment on the International Space Station. Above 80.5 GV the rigidity dependence of the cosmic ray Fe flux is identical to the rigidity dependence of the primary cosmic ray He, C, and O fluxes, with the Fe/O flux ratio being constant at 0.155 ± 0.006. This shows that unexpectedly Fe and He, C, and O belong to the same class of primary cosmic rays which is different from the primary cosmic rays Ne, Mg, and Si class.

DOI: 10.1103/PhysRevLett.126.041104

Primary iron cosmic rays are the most abundant heavy nuclei beyond silicon. They are thought to be mostly produced and accelerated in astrophysical sources. Iron interaction cross sections with the interstellar medium (p, He) are significantly larger than those of lighter nuclei (He, C, O, Ne, Mg, and Si). Therefore, iron nuclei interact much more with the interstellar medium during propagation. Precise knowledge of the iron spectrum in the GV–TV rigidity region provides important information on the origin, acceleration, and propagation processes of cosmic rays in the Galaxy [1]. Previously, the precision measurements of the primary cosmic ray He, C, and O fluxes and Ne, Mg, and Si fluxes with the Alpha Magnetic Spectrometer experiment (AMS) have been reported [2,3]. These measurements revealed an identical rigidity dependence of the He, C, and O fluxes above 60 GV and their deviation from a single power law (hardening) above ~200 GV. The AMS results also revealed unexpected differences in the rigidity dependence of the Ne, Mg,

and Si fluxes compared to the He, C, and O fluxes. To date, iron nuclei ($Z = 26$) are the highest charge cosmic rays measured by AMS. The rigidity dependence of the iron flux compared with that of lower-charge primary cosmic rays provides new insights into the origin and propagation of cosmic rays [4,5].

Over the last 30 years there have been many measurements of the Fe flux in kinetic energy per nucleon [6–17]. Typically these measurements have errors larger than 20% at 50 GeV/n (~100 GV in rigidity). There are no measurements of Fe flux in rigidity.

In this Letter we report the precise measurement of the Fe flux in the rigidity range from 2.65 GV to 3.0 TV based on 0.62×10^6 iron nuclei collected by AMS during the first 8.5 years (May 19, 2011 to October 30, 2019) of operation aboard the International Space Station (ISS). The total flux error is 4.8% at 100 GV.

Detector.—The layout and description of the AMS detector are presented in Ref. [18]. The key elements used in this measurement are the permanent magnet [19], the nine layers silicon tracker [20], $L1$-$L9$, and the four planes of time of flight TOF scintillation counters [21]. AMS also contains a transition radiation detector, a ring imaging Čerenkov detector, an electromagnetic calorimeter, and an array of 16 anticoincidence counters. Further details on the detector, trigger, and Monte Carlo (MC) simulation are contained in Refs. [22–24] and in the Supplemental Material [25].

Event selection.— In the first 8.5 yr AMS has collected 1.50×10^{11} cosmic ray events. Iron events are required to be downward going and to have a reconstructed track in the inner tracker which passes through $L1$. In the highest rigidity region, $R \geq 1.2$ TV, the track is also required to pass through $L9$. Charge measurements on $L1$, the inner tracker, the upper TOF, and, for $R > 1.2$ TV, the lower TOF, and $L9$ are required to be compatible with charge $Z = 26$, namely, $23.2 < Z_{L1} < 27.6$, $24.7 < Z_{\mathrm{UTOF}} < 27.6$, $25.5 < Z_{\mathrm{InnerTracker}} < 26.5$, $Z_{\mathrm{LTOF}} > 24.7$, $24.6 < Z_{L9} < 28.8$. Details of the event selection are contained in Refs. [23,26–29] and in the Supplemental Material [25].

The event selection yields purities of $> 97\%$ over the entire rigidity range. The impurities have two sources. The main source is a residual background from Mn nuclei due to the finite AMS charge resolution. It has been estimated as a function of rigidity by selecting events with tight charge cuts on $L1$ and upper and lower TOF and found to be less than 3% over the entire rigidity range, see Fig. S2 of the Supplemental Material [25]. The second source is the residual background from the interactions of heavy nuclei such as Co and Ni in the AMS materials above $L2$. It is negligible, $< 0.3\%$, over the entire rigidity range, as shown in Fig. S3 of the Supplemental Material [25].

After background subtraction we obtain 0.62×10^6 iron nuclei. The uncertainty due to background subtraction is $< 0.7\%$ independent of rigidity. It was estimated by varying the purity of the Fe sample from 95% to 99% and also by taking into account the statistical and systematic uncertainties in the template fit, see Fig. S3 of the Supplemental Material [25].

Data analysis.—The isotropic flux Φ_i in the ith rigidity bin $(R_i, R_i + \Delta R_i)$ is given by

$$\Phi_i = \frac{N_i}{A_i \epsilon_i T_i \Delta R_i}, \tag{1}$$

where N_i is the number of events corrected for bin-to-bin migration, A_i is the effective acceptance including geometric acceptance, event reconstruction and selection efficiencies, and inelastic interactions of nuclei in the AMS materials, as described below, ϵ_i is the trigger efficiency, and T_i is the collection time. In this Letter the flux was measured in 49 bins from 2.65 GV to 3.0 TV, with bin widths chosen according to the rigidity resolution and available statistics.

The bin-to-bin migration of events was corrected using the unfolding procedure described in Ref. [26]. These corrections, $(N_i - \aleph_i)/\aleph_i$ where $\aleph_i$ is the number of observed events in bin i, are $+33\%$ at 3 GV decreasing smoothly to $+11\%$ at 10 GV, $+2\%$ at 80 GV, $+1\%$ at 150 GV, and -2% at 3 TV.

Extensive studies were made of the systematic errors. These errors include the uncertainties in the background evaluation discussed above, the trigger efficiency, the geomagnetic cutoff factor, the acceptance calculation, the rigidity resolution function, and the absolute rigidity scale.

The systematic error on the fluxes associated with the trigger efficiency measurement is $< 1\%$ over the entire rigidity range.

The geomagnetic cutoff factor was varied from 1.0 to 1.4, resulting in a negligible systematic uncertainty ($<0.1\%$) in the rigidity range below 30 GV.

The effective acceptances A_i were calculated using MC simulation and corrected for small differences between the data and simulated events related to (a) event reconstruction and selection, namely in the efficiencies of velocity vector determination, track finding, charge determination, and tracker quality cuts and (b) the details of inelastic interactions of nuclei in the AMS materials. The total corrections to the effective acceptance from the differences between data and MC simulation were found to be $<5\%$ over the entire rigidity range. The systematic error on the flux associated with the reconstruction and selection is $<1\%$ over the entire rigidity range.

The material traversed by nuclei from the top of AMS to $L9$ is composed primarily of carbon and aluminum. The survival probabilities of Fe nuclei due to interactions in the materials were measured using cosmic ray data collected by AMS as described in Ref. [30]. The simulation of nuclear interactions has been validated with data using all AMS measured nuclear charge changing cross sections (Fe $\rightarrow$ He...Mn + X). Figure S4a of the Supplemental

Material [25] shows three examples $Fe \to Cr + X$, $Fe \to Si + X$, and $Fe \to O + X$; Fig. S4b shows the comparison between the simulated and measured Fe survival probabilities between $L1$ and $L2$ in TRD and upper TOF; Fig. S5 shows the nuclei inelastic cross section of He, B, C, N, O, Ne, Mg, Si, S, and Fe on a C target measured by AMS at 15 GV rigidity as a function of nuclei charge radius [31]. The systematic error due to uncertainties in the evaluation of the inelastic cross section is $< 4\%$ up to 100 GV. Above 100 GV, the small rigidity dependence of the cross section from the Glauber-Gribov model [24] was treated as an uncertainty and added in quadrature to the uncertainties from the measured interaction probabilities [30]. Therefore, the corresponding systematic errors on the Fe flux is $< 4\%$ up to 100 GV and rises smoothly to 4.5% at 3 TV.

The rigidity resolution function for Fe has a pronounced Gaussian core characterized by width σ and non-Gaussian tails more than 2.5σ away from the center [23]. Figure S6 of Supplemental Material [25] shows the complete AMS rigidity resolution function as smearing matrices for the $L1$-$L8$ and $L1$-$L9$ configurations. The resolution function has been verified with the procedures described in detail in Ref. [27]. The systematic error on the flux due to the rigidity resolution function was obtained by repeating the unfolding procedure while varying the width of the Gaussian core of the resolution function by 5% and by independently varying the amplitude of the non-Gaussian tails by 10% [23]. The resulting systematic error on the flux is less than 1% below 300 GV and smoothly increases to 2.5% at 3 TV.

There are two contributions to the systematic uncertainty on the rigidity scale [26]. The first is due to residual tracker misalignment. This error was estimated by comparing the E/p ratio for electrons and positrons, where E is the energy measured with the ECAL and p is the momentum measured with the tracker. It was found to be $1/30\ \mathrm{TV}^{-1}$ [32]. The second systematic error on the rigidity scale arises from the magnetic field map measurement and its temperature corrections [26]. The error on the Fe flux due to uncertainty on the rigidity scale is $< 1\%$ up to 300 GV and increases smoothly to 6% at 3 TV.

Most importantly, several independent analyses were performed on the same data sample by different study groups. The results of those analyses are consistent with this Letter.

Results.—The measured Fe flux including statistical and systematic errors is reported in Table SI of Supplemental Material [25] as a function of the rigidity at the top of the AMS detector. Figure 1(a) shows the Fe flux as a function of rigidity $\tilde{R}$ with the total errors, the sum in quadrature of statistical and systematic errors. In the figure the points are placed along the abscissa at $\tilde{R}$ calculated for a flux $\propto R^{-2.7}$ [33]. For comparison, Fig. 1(a) also shows our latest results on the oxygen flux from Refs. [2,34]. To examine the

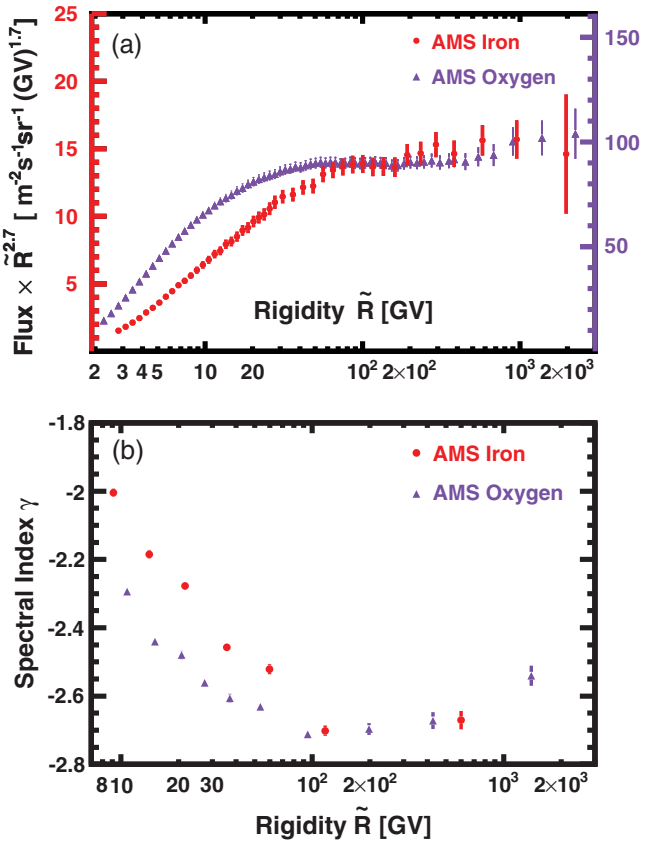

FIG. 1. (a) The AMS iron flux (red dots) and oxygen flux (violet triangles) multiplied by $\tilde{R}^{2.7}$ with total errors as a function of rigidity. (b) The AMS iron flux spectral index (red dots) and oxygen flux spectral index (violet triangles) dependence on rigidity. As seen, above 80.5 GV the rigidity dependence of the iron flux and spectral index follow the rigidity dependence of the oxygen flux and spectral index.

rigidity dependence of the Fe flux, the variation of the flux spectral indices with rigidity was obtained in a model independent way from

$$\gamma = d[\log(\Phi)]/d[\log(R)] \tag{2}$$

over nonoverlapping rigidity intervals bounded by 7.09, 12.0, 16.6, 28.8, 45.1, 80.5, 175.0, and 3000.0 GV. The results are presented in Fig. 1(b) together with the spectral index of the oxygen flux from Ref. [34]. As seen from Fig. 1, above 80.5 GV the iron flux and spectral index follow the oxygen flux and spectral index, with the iron flux behavior being consistent with the observed hardening of the oxygen flux.

Figure 2 shows the AMS iron flux as a function of kinetic energy per nucleon E_K together with earlier measurements [6,7,9–16]. Data from other experiments have been extracted using Ref. [35].

To compare the rigidity dependence of the Fe flux with that of He, C, and O primary cosmic ray fluxes, which have

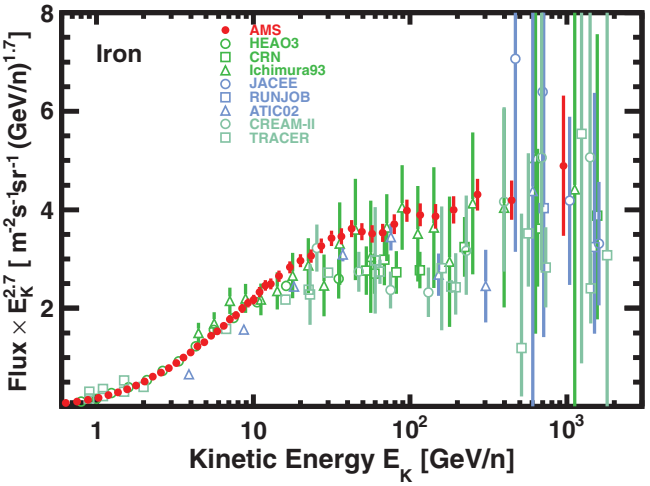

FIG. 2. The AMS iron flux as a function of kinetic energy per nucleon E_K multiplied by $E_K^{2.7}$ together with earlier measurements [6,7,9–16]. For the AMS measurement $E_K = (\sqrt{Z^2\tilde{R}^2 + M^2} - M)/A$ where Z, M, and A are the $^{56}_{26}$Fe nuclear charge, mass, and atomic mass numbers, respectively.

identical rigidity dependence above 60 GV [2,34], the ratio of the iron flux to the oxygen flux [34], Fe/O, was computed and is reported in Table SII of the Supplemental Material [25]. To compare the AMS result with previous measurements, the Fe/O ratio was converted from rigidity to kinetic energy per nucleon using the procedure described in Ref. [27]. Figure S7 of the Supplemental Material [25] shows the AMS Fe/O flux ratio as a function of kinetic energy per nucleon together with earlier measurements [6,7,11,13,15,16]. As seen, the AMS result provides an accurate functional energy dependence of the Fe/O flux ratio.

Figure 3(a) shows the AMS Fe/O ratio as a function of rigidity with total errors together with a constant value fit above 80.5 GV. The fit yields Fe/O $= 0.155 \pm 0.006$ with χ^2/d.o.f. $= 8/11$. This, together with Fig. 1, shows that Fe belongs to the same class of primary cosmic rays as He, C, and O.

Figure 3(b) shows the comparison of the Fe/O flux ratio with the cosmic ray propagation model GALPROP [36] prediction based on data available before AMS and with the latest GALPROP and HELMOD model [37] prediction based on published AMS data without including data in this Letter. As seen from Fig. 3(b), neither of these two models describes our data.

Cosmic ray nuclei fragment during their propagation in the Galaxy. Because of their different inelastic cross sections with the interstellar media, the fraction of nuclei which fragments at a given rigidity is different for iron and oxygen [38,39]. This, together with the propagation time (or Galactic leakage rate) rigidity dependence may significantly affect the measured Fe/O flux ratio [37]. Historically, there are several simple models describing the

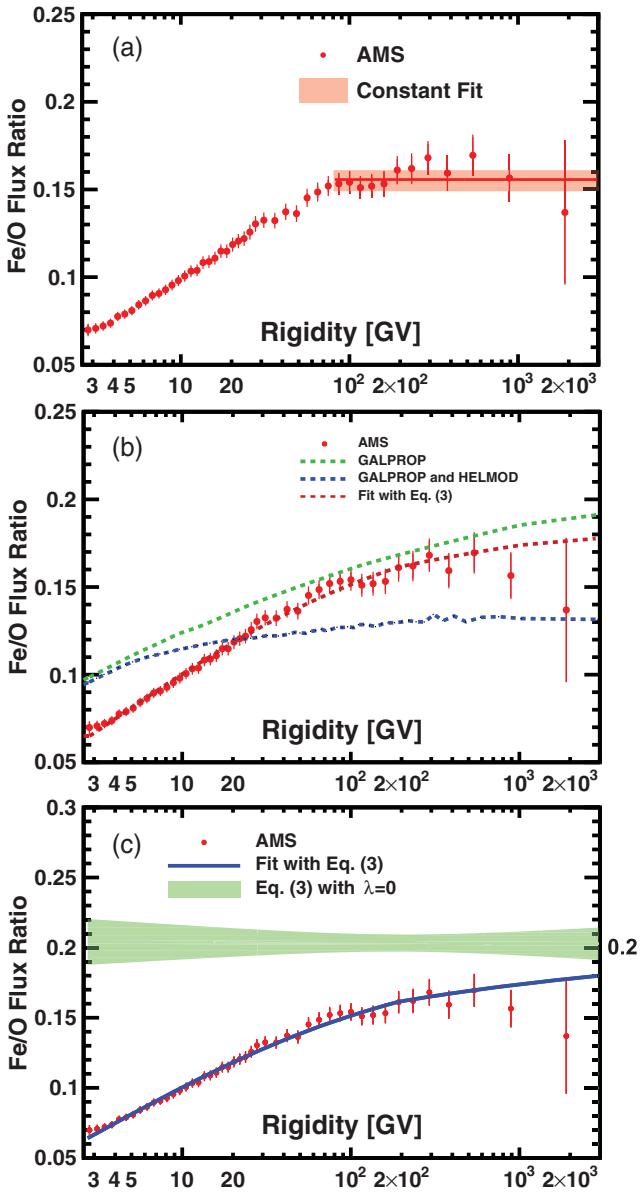

FIG. 3. The AMS Fe/O ratio as a function of rigidity with total errors and with (a) red band (1σ) indicating the constant value fit (Fe/O $= 0.155 \pm 0.006$ with χ^2/d.o.f. $= 8/11$) above 80.5 GV; b) dashed green curve, showing the prediction of the Fe/O ratio by the GALPROP model [36] based on data available before AMS and dashed blue curve showing the prediction of the Fe/O ratio by the latest GALPROP and HELMOD model [37] based on published AMS data without including data in this Letter; and (c) blue curve, showing the fit results with Eq. (3), and green band, showing the Fe/O flux ratio at the source, i.e., fit results of Eq. (3) with $\lambda = 0$.

propagation of primary cosmic ray nuclei through the interstellar medium such as the "slab" and the "leaky-box" models. In the slab model cosmic rays of a given rigidity traverse an equal amount of matter. In the leaky-box model the amount of matter traversed by cosmic rays of a given rigidity is distributed exponentially [40].

To assess the overall Fe/O flux ratio rigidity dependence at the source, before propagation, we have fitted it over the entire rigidity range using the slab model, $e^{-\lambda_S(\tilde{\sigma}_A-\tilde{\sigma}_{A'})}$, describing the propagation of primary nuclei through the interstellar medium [40] together with a source term $k(R/192\ \mathrm{GV})^{\Delta}$:

$$\frac{\Phi_A}{\Phi_{A'}} = k\left(\frac{R}{192\ \mathrm{GV}}\right)^{\Delta} e^{-\lambda_S(\tilde{\sigma}_A-\tilde{\sigma}_{A'})}, \tag{3}$$

where $\Phi_A/\Phi_{A'}$ is the flux ratio of primary nuclei A and A', k is a normalization factor, Δ is the flux ratio spectral index at the source,

$$\lambda_S = \begin{cases} \lambda(R/192\ \mathrm{GV})^{-0.38\pm0.02} & R \le 192\ \mathrm{GV} \\ \lambda(R/192\ \mathrm{GV})^{-0.24\pm0.03} & R > 192\ \mathrm{GV} \end{cases} \tag{4}$$

is a mean material grammage ($\mathrm{g\,cm^{-2}}$) with rigidity dependence from Refs. [4,34,41] and λ is the grammage at $R = 192$ GV,

$$\tilde{\sigma}_A = \frac{1-f}{m_p}\sigma^{A+p} + \frac{f}{m_{\mathrm{He}}}\sigma^{A+\mathrm{He}} \tag{5}$$

is the mass averaged cross section of a nucleus A, $f = 0.28 \pm 0.02$ is the helium mass fraction in the interstellar medium [42], m_p and m_{He} are the proton and ^{4}He masses, and σ^{A+p} and $\sigma^{A+\mathrm{He}}$ are the corresponding nuclei inelastic cross sections with protons and helium in the interstellar medium, respectively, evaluated using measurements from Refs. [39,43].

The fit parameters are k, Δ, and λ. The fit yields $k = 0.203 \pm 0.008$, $\Delta = -0.002 \pm 0.017$, and $\lambda = 1.04 \pm 0.11\ \mathrm{g\,cm^{-2}}$ with $\chi^2/\mathrm{d.o.f.} = 22/43$. The Fe/O flux ratio fit result is shown in Fig. 3(c). As seen, the Δ parameter is consistent with zero, which implies that in this model the Fe/O flux ratio at the source is constant over the entire rigidity range, as illustrated by the green band in Fig. 3(c). As seen, the model of Eq. (3) provides a good description of the Fe/O flux ratio. For completeness, we have also studied Eq. (3) with primary flux ratios Fe/He, He/O, and Fe/Si. The results are reported in the Supplemental Material [25] and shown in Table SA and Fig. S8 of the Supplemental Material [25]. As seen, the model of Eq. (3) also provides a good description of the Fe/He, He/O, and Fe/Si flux ratios. As seen in Fig. S8 of Supplemental Material [25], in the model the Fe/O, Fe/He, and He/O flux ratios at the source are constant over the entire rigidity range, however, the Fe/Si flux ratio at the source is not constant (at the 3σ level). The results of this model are consistent with the observation that He, O, and Fe belong to one class of primary cosmic rays and Si belongs to a different class.

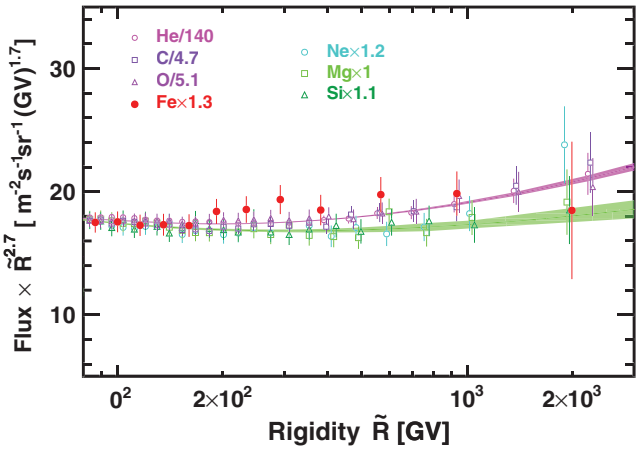

FIG. 4. The rigidity dependence of the Fe flux compared with the rigidity dependence of the He, C, and O fluxes and the Ne, Mg, and Si fluxes above 80.5 GV. For clarity, the He, O, Ne, and Si data points above 400 GV are displaced horizontally. For display purposes only, the He, C, O, Ne, Si, and Fe fluxes were rescaled as indicated. The shaded areas show the fit result of Eq. (5) of Ref. [3] to He, C, and O fluxes (magenta) and Ne, Mg, and Si fluxes (green).

We have also fitted the AMS Fe/O and Fe/Si flux ratios using the leaky box model [40]. The details are discussed in the Supplemental Material [25] and shown in Fig. S9. As seen, the leaky box model fails to describe the AMS results.

Most importantly, independent of any model [36,37,44], the measured rigidity dependence of Fe above 80.5 GV follows the rigidity dependence of O, see Fig. 1(a) and Fig. 3(a). Therefore as shown in Fig. 4, unexpectedly Fe belongs to the He, C, and O class of primary cosmic rays [2,34], which is different from the rigidity dependence of Ne, Mg, and Si [3].

In conclusion, we have presented the precision measurement of the Fe flux as a function of rigidity from 2.65 GV to 3.0 TV, with detailed studies of the systematic errors. Above 80.5 GV the rigidity dependence of the cosmic ray Fe flux is identical to the rigidity dependence of the primary cosmic ray He, C, and O class, which is different from the rigidity dependence of primary cosmic rays Ne, Mg, and Si class. In particular, above 80.5 GV the Fe/O ratio is well described by a constant value of 0.155 ± 0.006. These are new and unexpected properties of primary iron cosmic rays.

We are grateful for important physics discussions with Pasquale Blasi, Fiorenza Donato, Jonathan Feng, and Igor Moskalenko. We thank former NASA Administrator Daniel S. Goldin for his dedication to the legacy of the ISS as a scientific laboratory and his decision for NASA to fly AMS as a DOE payload. We also acknowledge the continuous support of the NASA leadership, particularly William H. Gerstenmaier, and of the JSC and MSFC flight control teams that have allowed AMS to operate optimally on the ISS for over nine years. We are grateful for the

support of Jim Siegrist, Glen Crawford, and their staff of the DOE including resources from the National Energy Research Scientific Computing Center under Contract No. DE-AC02-05CH11231. We gratefully acknowledge the strong support from CERN including Fabiola Gianotti, and the CERN IT department including Bernd Panzer-Steindel, and from the European Space Agency including Johann-Dietrich Wörner and Simonetta Di Pippo. We also acknowledge the continuous support from MIT and its School of Science, Michael Sipser, and the Laboratory for Nuclear Science, Boleslaw Wyslouch. Research supported by: Chinese Academy of Sciences, Institute of High Energy Physics, Institute of Electrical Engineering, China Academy of Space Technology, National Natural Science Foundation, and Ministry of Science and Technology, the China Scholarship Council, the Shandong, Jiangsu, and Guangdong provincial governments, Shandong University, and Shandong Institute of Advanced Technology, China; the Academy of Finland, Project No. 321882, Finland; CNRS/IN2P3 and CNES, France; Pascale Ehrenfreund, DLR under Grants No. 50OO1403 and 50OO1805 and JARA-HPC under Project No. JARA0052, Germany; INFN and ASI under ASI-INFN Agreements No. 2014-037-R.1-2017 and No. 2019-19-HH.0 and ASI-University of Perugia Agreement No. 2019-2-HH.0, Italy; CHEP and NRF under Grant No. NRF-2018R1A6A1A06024970 at Kyungpook National University, Korea; the Consejo Nacional de Ciencia y Tecnología and UNAM, Mexico; NWO under Grant No. 680-1-004, Netherlands; FCT under Grant No. CERN/FIS-PAR/0013/2019, Portugal; the Ministry of Science and Higher Education under Project No. 0723-2020-0040, Russia; CIEMAT, IAC, CDTI, and SEIDI-MINECO under Grants No. PID2019–107988 GB-C21/C22, No. CEX2019-000920-S, and No. MDM-2015-0509, Spain; the Swiss National Science Foundation (SNSF), federal and cantonal authorities, and the Fondation Dr. Manfred Steuer, Switzerland; Academia Sinica and the Ministry of Science and Technology (MOST) under Grants No. 107-2119-M-006-015-MY3, No. 109-2112-M-001-029, and No. CDA-105-M06, former Presidents of Academia Sinica Yuan-Tseh Lee and Chi-Huey Wong and former Ministers of MOST Maw-Kuen Wu and Luo-Chuan Lee, Taiwan; the Turkish Energy, Nuclear and Mineral Research Agency (TENMAK) under Grant No. 2020TAEK(CERN)A5.H1.F5-26, Turkey; and NSF Grants No. 1455202 and No. 1551980, Wyle Laboratories Grant No. 2014/T72497, and NASA NESSF Grant No. HELIO15F-0005, USA.

[*]Also at Nikhef, 1098 XG Amsterdam, Netherlands.
[†]Also at ASI Space Science Data Center (SSDC), 00133 Roma, Italy.
[‡]Also at Policlinico S. Orsola-Malpighi, 40138 Bologna, Italy.

[1] I. A. Grenier, J. H. Black, and A. W. Strong, Annu. Rev. Astron. Astrophys. **53**, 199 (2015); P. Blasi, Astron. Astrophys. Rev. **21**, 70 (2013); A. W. Strong, I. V. Moskalenko, and V. S. Ptuskin, Annu. Rev. Nucl. Part. Sci. **57**, 285 (2007); A. Castellina and F. Donato, Astropart. Phys. **24**, 146 (2005).
[2] M. Aguilar *et al.*, Phys. Rev. Lett. **119**, 251101 (2017).
[3] M. Aguilar *et al.*, Phys. Rev. Lett. **124**, 211102 (2020).
[4] G. Jóhannesson *et al.*, Astrophys. J. **824**, 16 (2016).
[5] M. J. Boschini *et al.*, Astrophys. J. **840**, 115 (2017); **858**, 61 (2018).
[6] J. J. Engelmann *et al.*, Astron. Astrophys. **233**, 96 (1990).
[7] S. P. Swordy, D. Müller, P. Meyer, J. L'Heureux, and J. M. Grunsfeld, Astrophys. J. **374**, 356 (1991).
[8] J. A. Esposito *et al.*, Astropart. Phys. **1**, 33 (1992).
[9] M. Ichimura, M. Kogawa, S. Kuramata, H. Mito, and T. Murabayashi *et al.*, Phys. Rev. D **48**, 1949 (1993).
[10] Y. Takahashi Nucl. Phys. B, Proc. Suppl. **60**, 83 (1998); T. A. Parnell *et al.*, Adv. Space Res. **9**, 45 (1989).
[11] F. Gahbauer, G. Hermann, J. R. Hörandel, D. Müller, and A. A. Radu, Astrophys. J. **607**, 333 (2004).
[12] V. A. Derbina *et al.*, Astrophys. J. **628**, L41 (2005).
[13] M. Ave, P. J. Boyle, F. Gahbauer, C. Höppner, J. R. Hörandel, M. Ichimura, D. Müller, and A. Romero-Wolf, Astrophys. J. **678**, 262 (2008).
[14] A. D. Panov *et al.*, Bull. Russ. Acad. Sci. **73**, 564 (2009).
[15] H. S. Ahn *et al.*, Astrophys. J. **715**, 1400 (2010); **707**, 593 (2009).
[16] A. Obermeier, M. Ave, P. J. Boyle, C. Höppner, J. R. Hörandel, and D. Müller, Astrophys. J. **742**, 14 (2011).
[17] K. A. Lave *et al.*, Astrophys. J. **770**, 117 (2013); J. S. George *et al.*, Astrophys. J. **698**, 1666 (2009).
[18] A. Kounine, Int. J. Mod. Phys. E **21**, 1230005 (2012); S. Rosier-Lees, in *Proceedings of Astroparticle Physics TEVPA/IDM, Amsterdam, 2014* (unpublished); S. Ting, Nucl. Phys. B, Proc. Suppl. **243–244**, 12 (2013); S.-C. Lee, in *Proceedings of the 20th International Conference on Supersymmetry and Unification of Fundamental Interactions (SUSY 2012), Beijing, 2012* (unpublished); M. Aguilar, in *Proceedings of the XL International Meeting on Fundamental Physics, Centro de Ciencias de Benasque Pedro Pascual, 2012* (unpublished); S. Schael, in *Proceedings of the 10th Symposium on Sources and Detection of Dark Matter and Dark Energy in the Universe, Los Angeles, 2012* (unpublished); B. Bertucci, *Proc. Sci.*, EPS-HEP2011 (2011) 67; M. Incagli, AIP Conf. Proc. **1223**, 43 (2010); R. Battiston, Nucl. Instrum. Methods Phys. Res., Sect. A **588**, 227 (2008).
[19] K. Lübelsmeyer *et al.*, Nucl. Instrum. Methods Phys. Res., Sect. A **654**, 639 (2011).
[20] B. Alpat *et al.*, Nucl. Instrum. Methods Phys. Res., Sect. A **613**, 207 (2010).
[21] V. Bindi *et al.*, Nucl. Instrum. Methods Phys. Res., Sect. A **743**, 22 (2014).
[22] G. Ambrosi, V. Choutko, C. Delgado, A. Oliva, Q. Yan, and Y. Li, Nucl. Instrum. Methods Phys. Res., Sect. A **869**, 29 (2017).
[23] M. Aguilar *et al.*, Phys. Rev. Lett. **115**, 211101 (2015).
[24] J. Allison *et al.*, Nucl. Instrum. Methods Phys. Res., Sect. A **835**, 186 (2016); J. Allison *et al.*, IEEE Trans. Nucl. Sci. **53**,

270 (2006); S. Agostinelli *et al.*, Nucl. Instrum. Methods Phys. Res., Sect. A **506**, 250 (2003).

[25] See Supplemental Material at http://link.aps.org/supplemental/10.1103/PhysRevLett.126.041104 for details on the detector, event selection, further study and tabulated results of the "slab" model, Eq. (3), a study of the "leaky box" model, Eq. (6), the tabulated Fe flux and the Fe/O, Fe/He, and Fe/Si flux ratios all as functions of rigidity; and figures regarding rigidity resolution, charge selection, systematic errors, the Fe on C nuclei cross section measurement, the AMS Fe/O flux ratio as a function of kinetic energy together with earlier measurements, and AMS Fe/O, Fe/He, He/O, and Fe/Si flux ratios together with fits of Eq. (3) and, for Fe/O and Fe/Si, fits of Eq. (6).

[26] M. Aguilar *et al.*, Phys. Rev. Lett. **114**, 171103 (2015).

[27] M. Aguilar *et al.*, Phys. Rev. Lett. **117**, 231102 (2016).

[28] J. Alcaraz *et al.*, Phys. Lett. B **484**, 10 (2000).

[29] C. C. Finlay *et al.*, Geophys. J. Int. **183**, 1216 (2010); E. Thébault *et al.*, Earth Planets Space **67**, 79 (2015); Geomagnetic Field Modeling Working Group, IGRF-13 model, https://www.ngdc.noaa.gov/IAGA/vmod/igrf.html (2019).

[30] Q. Yan, V. Choutko, A. Oliva, and M. Paniccia, Nucl. Phys. **A996**, 121712 (2020).

[31] I. Angeli and K. P. Marinova, At. Data Nucl. Data Tables, **99**, 69 (2013).

[32] J. Berdugo, V. Choutko, C. Delgado, and Q. Yan, Nucl. Instrum. Methods Phys. Res., Sect. A **869**, 10 (2017).

[33] G. D. Lafferty and T. R. Wyatt, Nucl. Instrum. Methods Phys. Res., Sect. A **355**, 541 (1995). We have used Eq. (6) with $\tilde{R} \equiv x_{lw}$.

[34] M. Aguilar *et al.*, Phys. Rep. (to be published), https://doi.org/10.1016/j.physrep.2020.09.003.

[35] D. Maurin, F. Melot, and R. Taillet, Astron. Astrophys. **569**, A32 (2014).

[36] We used GALPROP WebRun, A. E. Vladimirov, S. W. Digela, G. Jóhannesson, P. F. Michelson, I. V. Moskalenko, P. L. Nolan, E. Orlando, T. A. Porter, and A. W. Strong, Comput. Phys. Commun. **182**, 1156 (2011); with parametrization from R. Trotta, G. Jóhannesson, I. V. Moskalenko, T. A. Porter, R. Ruiz de Austri, and A. W. Strong, Astrophys. J. **729**, 106 (2011).

[37] M. J. Boschini *et al.*, Astrophys. J. Suppl. Ser. **250**, 27 (2020).

[38] C. Evoli, R. Aloisio, and P. Blasi, Phys. Rev. D **99**, 103023 (2019).

[39] W. R. Webber, J. C. Kish, and D. A. Schrier, Phys. Rev. C **41**, 520 (1990).

[40] M. S. Longair, *High Energy Astrophysics*, 3rd ed. (Cambridge University Press, Cambridge, England, 2011), p. 507.

[41] M. Aguilar *et al.*, Phys. Rev. Lett. **120**, 021101 (2018).

[42] Y. I. Izotov and T. X. Thuan, Astrophys. J. Lett. **710**, L67 (2010); A. W. Strong and I. V. Moskalenko, Astrophys. J. **509**, 212 (1998).

[43] V. V. Glagolev *et al.*, Z. Phys. C **60**, 421 (1993).

[44] A. Putze, D. Maurin, and F. Donato, Astron. Astrophys. **526**, A101 (2011).